


RESEARCH ARTICLE

Open Access



Development of a toxin-selective immunotracer for in vivo detection of *Clostridioides difficile* infection by immunoPET

Mario González-Arjona^{1†}, Lorena Cussó^{1,2,3†}, Luis Alcalá^{4,5,6}, María Isabel González², Alexandra de Francisco^{1,2,3}, María Jesús Fernández-Aceñero^{7,10}, Dag Sehlin⁸, Stina Syvänen⁸, Emilio Bouza^{4,5,6}, Patricia Muñoz^{4,5,6}, Manuel Desco^{1,2,3,9*} and Beatriz Salinas^{1,2,3,9*} 

[†]Mario González-Arjona and Lorena Cussó have contributed equally to this work.

*Correspondence: desco@hggm.es; beatriz.salinas@uc3m.es

¹ Unidad de Medicina y Cirugía Experimental, Hospital General Universitario Gregorio Marañón, Instituto de Investigación Sanitaria Gregorio Marañón, 28007 Madrid, Spain

⁹ Department of Bioengineering, Universidad Carlos III de Madrid, 28911 Madrid, Spain
Full list of author information is available at the end of the article

Abstract

Background: *Clostridioides difficile* infection (CDI) is a major healthcare challenge that is associated with high morbidity and mortality. Current diagnostic methods are limited in terms of specificity and invasiveness, necessitating novel, non-invasive imaging techniques. In this study, we develop and evaluate an immunoPET radiotracer targeting *C. difficile* toxin B for in vivo detection of CDI in a murine model.

Results: The monoclonal antibody bezlotoxumab, was radiolabeled with [¹²⁵I] for in vitro characterization and with [⁸⁹Zr]Zr for in vivo PET imaging, resulting in high radiochemical yields (75.36 ± 4.11% for [¹²⁵I] and 71.58 ± 8.19% for [⁸⁹Zr]Zr) and purities (> 99.99% in both cases), with stable binding properties. PET/CT imaging 48 h post-infection in an animal model of CDI (C57BL/6 mice and ribotype 027 strain) demonstrated specific accumulation of [⁸⁹Zr]Zr-DFO-Beztaxab in the colon and cecum of infected mice, thus making it possible to distinguish CDI from dysbiosis without specific *C. difficile* infection and healthy controls. Findings were confirmed by PET-based quantification and ex vivo biodistribution.

Conclusions: We successfully developed an immunoPET radiotracer targeting toxin B for detection of CDI. Its application in an animal CDI model proved its capacity to detect the source of infection with high specificity, while avoiding confusion with non-specific inflammation.

Keywords: *Clostridioides difficile*, ImmunoPET, Bacterial toxin targeting, Imaging of infection, Radiotracer development

Background

Clostridioides difficile (*C. difficile*) infection (CDI) remains a persistent and formidable challenge in healthcare facilities worldwide, generating a significant burden in terms of patient health outcomes, healthcare resources, and infection control (Czepiel et al. 2019). It is the leading cause of hospital-acquired infections in US hospitals (Rose et al. 2023) and has a high prevalence in European hospitals, accounting for 7.3% of all hospital-acquired infections (Szabó et al. 2022). CDI is associated with significant morbidity

and mortality, which are exacerbated by its propensity for recurrent infections and complications such as pseudomembranous colitis and toxic megacolon (Czepiel et al. 2019). Despite advances in prevention and control of infection, the incidence and severity of CDI continue to rise, underscoring the urgent need for innovative diagnostic and therapeutic approaches to effectively manage this escalating public health problem (Viprey et al. 2022).

The most commonly used diagnostic strategy for CDI follows an algorithm that begins with initial screening based on an enzyme immunoassay (EIA) to detect the enzyme glutamate dehydrogenase (GDH), which is highly sensitive for CDI (Gilligan 2008). Since both toxigenic and non-toxigenic strains of *C. difficile* produce GDH, a positive GDH result in EIA requires confirmatory testing. This confirmation typically involves real-time PCR targeting the toxin B gene, with or without an intermediate EIA for the detection of toxins A and B. The intermediate EIA aims to reduce the overall cost of molecular testing. This diagnostic algorithm has been extensively evaluated in multiple studies, demonstrating a sensitivity of 85–90% and a specificity exceeding 99% compared to toxigenic culture, the previous gold standard for diagnosis of CDI (McDonald et al. 2018; Novak-Weekley et al. 2010; Crobach et al. 2009; Bocchetti et al. 2023).

Although this approach is widely adopted in clinical practice, it is not without limitations. The associated challenges are particularly evident in cases where toxin concentrations are low, as patients may not have CDI but instead be asymptomatic carriers of toxigenic *C. difficile*. Colonoscopy, which would enable direct observation of the damage caused by the microorganism in the colon, is not recommended for severely ill patients because it significantly increases the risk of perforation. These tests are highly invasive and require the patient to be sedated, thus entailing specific risks and side effects (Cho et al. 2020; Fujitani et al. 2011). The challenges associated with CDI highlight the inadequacies of current diagnostic procedures and underscore the need for more accurate and reliable diagnostic tools.

Molecular imaging techniques have emerged as promising additions to conventional diagnostic approaches, offering the potential for non-invasive visualization and characterization of infectious diseases. Radiological techniques, including radiography, ultrasound, computed tomography (CT), and magnetic resonance imaging, are frequently used, especially to identify cases of toxic megacolon. However, these purely structural imaging tools rely on anatomic or morphologic changes that often occur after molecular events in the disease process, thereby precluding early detection of the infection. Furthermore, they are nonspecific and may reflect a combination of infection and host inflammatory response (Fujitani et al. 2011; Frickenstein et al. 2019; Guerri et al. 2019; Paláu-Dávila et al. 2016).

Nuclear imaging modalities such as positron emission tomography (PET) and single photon emission computed tomography (SPECT) have been investigated for their utility in diagnosing CDI by targeting the metabolic processes associated with bacterial infection. Among these, PET imaging with [¹⁸F]F-fluorodeoxyglucose ([¹⁸F]F-FDG) has attracted considerable interest owing to its ability to detect areas of increased glucose metabolism characteristic of infectious foci (Casali et al. 2021). Our group has pioneered its application to detect and evaluate CDI in a mouse model (Cusso et al. 2020), where

we analyzed [^{18}F]F-FDG uptake in the abdomen in models infected with two *C. difficile* ribotypes of different virulence.

[^{18}F]F-FDG enters leukocytes, macrophages, and CD4-positive T cells at infection sites (Ishimori et al. 2002), making it impossible to differentiate between infectious, inflammatory, and tumor lesions, and even organs with high basal metabolism. This can lead to confusion when foci are close to organs such as the heart or brain due to the natural glucose uptake in those organs, or to false positives due to non-specific uptake in non-infectious inflammatory processes (Bertagna et al. 2012; Rosenbaum et al. 2006). These limitations restrict its potential use, highlighting the need for more specific imaging probes.

To address these challenges and improve diagnostic accuracy in CDI, our research efforts aim to develop a novel molecular imaging approach that combines the specificity of targeted molecular therapy with the sensitivity of radiotracer imaging. Our proposed strategy involves radiolabeling a commercially available monoclonal antibody, bezlotoxumab, with the radionuclide [^{89}Zr]Zr to create a customized radiotracer, tailored for the detection of *C. difficile* toxins. Bezlotoxumab targets and neutralizes *C. difficile* toxin B, thus providing an opportunity for targeted molecular imaging owing to its high affinity and selectivity (Wilcox et al. 2017). By using this radiolabeled antibody in an animal model, we aim to explore the possibility of selectively targeting active CDI within the host, enabling precise localization and visualization of affected sites. All phases of this project have been designed in accordance with the recommendations published by A. Signore et al. (Alberto et al. 2023) for the development of new radiotracers to target bacterial infections.

Materials and methods

Unless otherwise specified, all reagents were purchased from Merck (KGaA, Darmstadt, Germany) and used without further purification.

Radiolabeling of commercial bezlotoxumab and physico-chemical characterization

Commercial bezlotoxumab (Merck & Co., Inc., Rahway, NJ, USA) was radiolabeled with two different radionuclides: [^{125}I]I for in vitro binding and kinetics studies, and [^{89}Zr]Zr for physicochemical characterization, and in vivo and ex vivo studies. Both radioisotopes were purchased from Revvity, Inc. (Waltham, MA, USA). For both immunoconjugates, radiochemical yield was estimated as the fraction of purified radiotracer activity compared to the initial amount of activity (%). Specific activity was calculated as the final radioactivity of radiotracer per milligram of antibody (MBq/mg).

Synthesis and physico-chemical characterization of [^{125}I]I-Beztxab

Radioiodination of bezlotoxumab was performed following the traditional direct labeling method (Gustavsson et al. 2023). Briefly, 20 μg of bezlotoxumab (8 μL) was mixed with 95 μL of phosphate-buffered saline (PBS) 1 \times and 2 μL [^{125}I]I (2.00–2.52 MBq). The reaction was started by adding 5 μL of a 1-mg/mL solution of chloramine-T trihydrate and incubated at room temperature for 90 s. Then, 10 μL of a 1-mg/mL solution of sodium metabisulfite was added to stop the reaction, and the radiolabeled antibody was isolated

using Zeba™ Spin Desalting Columns with a molecular weight cut-off of 7 K (Thermo Fisher Scientific, Waltham, MA, USA).

The purity of the radiotracer was evaluated using instant thin layer chromatography (iTLC) with silica gel (SG) chromatographic paper (Agilent Technologies, Inc., Santa Clara, CA, USA) as the stationary phase and acetone 70% as the mobile phase.

Loss of protein was determined using indirect enzyme-linked immunosorbent assay (ELISA) with an anti-human IgG (Fc-specific) antibody and labeled and unlabeled Beztxab and calculated using a 4PL nonlinear regression model.

Synthesis and physico-chemical characterization of [⁸⁹Zr]Zr-DFO-Beztxab

For the labeling of the mAb with the radiometal [⁸⁹Zr]Zr, bezlotoxumab was first conjugated to the isothiocyanatobenzyl-derivative of the chelator desferrioxamine (p-NCS-Bz-DFO, Chematech, Dijon, France) by adapting the labeling approach from previous works (Vosjan et al. 2010; Zeglis and Lewis 2015). Briefly, 1 mg of bezlotoxumab (40 μL) was adjusted to 1 mL with 0.1 M sodium bicarbonate buffer (pH = 9.0). In parallel, 1 mg of p-NCS-Bz-DFO was diluted in 200 μL of dimethyl sulfoxide, and 20 μL was added to the antibody solution in four additions of 5 μL, with gentle mixing between the additions. The mixture was incubated at 37°C, 500 rpm for 30 min in an Eppendorf® ThermoMixer® C (Eppendorf, Hamburg, Germany). Conjugated antibody was purified using a PD-10 desalting column (GE Healthcare Bio-Science AB, Chicago, IL, USA) and collected in 2 mL of HEPES buffer 0.5 M.

The ratio of p-DFO-Bz-NCS to bezlotoxumab was measured using MALDI-TOF MS/MS (Unidad de Espectrometría de Masas, Universidad Complutense de Madrid, Spain) following previous publications (Price et al. 2017). Briefly, unconjugated antibody (bezlotoxumab, 1-μL aliquot), p-DFO-Bz-NCS, and Bz-DFO-Beztxab were combined with an equal volume of sinapic acid, which was used as the matrix solution (10 mg/mL in 50% acetonitrile, 50% water, and 0.1% trifluoroacetic acid). Samples were then deposited onto a stainless-steel target plate and left to dry. Following the determination of the mass (m/z) of both the unaltered antibody and the immunoconjugate, the difference was divided by the chelator's molecular weight, and the p-DFO-Bz-NCS:bezlotoxumab ratio was expressed as the number of chelates per antibody unit.

For radiolabeling, oxalic acid 1 M was added to 74–111 MBq of [⁸⁹Zr]Zr-oxalic acid solution to a final volume of 2 mL. Then, 90 μL of sodium carbonate 2 M was added, and the mixture was incubated at room temperature, 500 rpm for 3 min in the ThermoMixer. Next, 300 μL of HEPES 0.5 M, 710 μL of Bz-DFO-Beztxab and 700 μL of HEPES 0.5 M were added to the mixture and kept in the reaction for 60 min at room temperature and 500 rpm in the ThermoMixer. Lastly, radiolabeled antibody was purified using 100 kDa Amicon filters (centrifuged at 4°C/21884 rcf/10 min, recovered at 4°C/5471 rcf/5 min).

Purity was evaluated using iTLC with Whatmann™ strips (3 MM CHR; GE Healthcare Bio-Science AB, Chicago, IL, USA) as the stationary phase, and citric acid monohydrate/sodium carbonate (pH 4.9–5.1) as the mobile phase. The radioactivity of the TLC plates was read using a miniGita Single system (Elisa-Raytest, Angleur, Belgium).

Radiolabeled-antibody mass was determined using the Bradford-Coomassie assay according to the manufacturer's instructions with a VICTOR Nivo Multimode Microplate Reader (Revvity, Inc., Waltham, MA, USA).

In vitro characterization

In vitro stability

In vitro stability of the radiotracers was evaluated in PBS 1× and mouse serum for [¹²⁵I]I-Beztxab and in PBS 1× for [⁸⁹Zr]Zr-DFO-Beztxab. Briefly, aliquots of [⁸⁹Zr]Zr-DFO-Beztxab (3.70 MBq) and [¹²⁵I]I-Beztxab (0.74 MBq) were added to 0.5–1 mL of PBS 1× and mouse serum, which had previously been tempered at 37°C with constant shaking. Samples were then collected at different time-points and analyzed using radio-TLC as described in the synthesis section.

- [⁸⁹Zr]Zr-DFO-Beztxab PBS 1× time-points: 0 h, 0.5 h, 1 h, 2 h, 4 h, 20 h, 26.5 h, 45 h, 51 h, 68 h, 74 h, 95 h and 100 h.
- [¹²⁵I]I-Beztxab PBS 1× and mouse serum time-points: 0 h, 0.25 h, 0.5 h, 1 h, 2 h, 4 h, 7 h, 24 h, 27 h, 30 h, 48 h, 51 h, 54 h, 72 h, 75 h, 78 h, 96 h, 100 h, 168 h, 192 h.

Hydrophobicity of [⁸⁹Zr]Zr-DFO-Beztxab

The hydrophobicity of the radiotracer was assessed using the partitioning method based on the LogP calculation. Briefly, 0.37 MBq of [⁸⁹Zr]Zr-DFO-Beztxab was added to an immiscible biphasic solution consisting of 500 µL of 1-octanol and 500 µL of PBS 1× (n = 3). This mixture was then incubated at 37 °C for 30 min with vigorous shaking and allowed to stand for a further 30 min to ensure proper phase separation. Finally, 100-µL samples were taken from each phase and their activity was measured using a Genesys gamma counter (Laboratory Technologies Inc., Elburn, IL, USA).

Binding kinetics for [¹²⁵I]I-Beztxab

Binding kinetics was measured using ELISA and LigandTracer (Wang et al. 2014).

ELISA: A 96-well half area clear flat bottom polystyrene high bind microplate (Corning Inc, Corning, NY, USA) was coated with 50 µL of 0.5 µg/mL *C. diff* Toxin B and left at 4 °C overnight. Wells were emptied, filled with 150 µL of ELISA Blocking Buffer (1% BSA, 0.15% Kathon ProClin™ 150 in PBS 1×, pH 7.4) and shaken at 900 rpm for 1 h. Then, wells were emptied and washed four times with ELISA Washing Buffer (NaH₂PO₄ × H₂O 0.32 mM, Na₂HPO₄ × 2H₂O 2.17 mM, NaCl 150 mM, 7.5 × 10⁻³% Kathon ProClin™ 150, 0.1% TWEEN® 20 in MQ water, pH 7.5). Next, 50 µL of unlabeled bezlotoxumab (n = 5) and [¹²⁵I]I-Beztxab (n = 3) was added to the plate in serial dilutions from 10 nM to 0.64 pM in ELISA Incubation Buffer (0.1% BSA, 0.15% Kathon ProClin™ 150, 0.05% TWEEN® 20 in PBS 1×, pH 7.4) and left at 4 °C overnight. The wells were then emptied and washed as described above and incubated with HRP-conjugated polyclonal goat anti-human-IgG-F(ab')₂ antibody (Jackson ImmunoResearch Laboratories, West Grove, PA, USA) diluted 1:2000 at 900 rpm for 1 h. Wells were emptied and washed, filled with 50 µL K Blue Aqueous TMB substrate (Neogen Corp., Lexington, KY, USA) and incubated for 5 min. The reaction was stopped by adding 50 µL of H₂SO₄ 1 M, and signal absorbance was read with a spectrophotometer at 450 nm. The equilibrium dissociation constant (K_D) was cal-

culated using a one site-specific binding non-linear regression. For calculations, the concentration of [125 I]I-Beztxab was corrected according to the percentage of protein loss calculated as described above.

LigandTracer: In a high-bind circular Petri dish (Corning Inc, Corning, NY, USA), 300 μ L of a 10 μ g/mL solution of *C. diff* Toxin B was added on a local spot at the edge of the dish. The dish was left tilted at 4 °C overnight. Then, the solution was removed, and the surface of the dish was blocked with ELISA blocking buffer for 1 h. Blocking buffer was removed, 2 mL of running buffer (0.1% BSA in PBS 1 \times) was added, and the dish was placed in the Ligand Tracer Grey instrument (Ridgeview Instruments AB, Uppsala, Sweden). Baseline was recorded for 15 min, running buffer was removed, and 2 mL of a 0.14–0.73 nM [125 I]I-Beztxab ($n = 3$) solution was added. Radioactivity at the coated spot and at a non-coated spot (association) was recorded for 3 h. Then, the concentration of [125 I]I-Beztxab was increased to 0.47–2.19 nM, and radioactivity was further recorded for 3 h. Lastly, [125 I]I-Beztxab solution was removed, the dish was washed with running buffer, and dissociation was recorded in 2 mL of running buffer for 72 h. Association (k_a), dissociation (k_d), and K_D rate constants were calculated with Trace Drawer 1.8.1 software (Ridgeview Instruments AB).

Toxin A and B quantification assay for *Clostridioides difficile* strains

Toxin of various *C. difficile* strains was quantified to identify the highest toxin-producing strain for use in our animal CDI model. The study was performed using *C. difficile* Toxin A/B FIA (SD Biosensor), a fluorescent immunoassay capable of measuring the fluorescence emitted by toxins A and B labeled with a fluorescent antibody. Three strains were included in this assay, namely, ATCC 43255 (ribotype 087), strain 14243227 (ribotype 027), and strain 13061479 (ribotype 001). These strains were previously employed by our team in a study on CDI using a mouse model (Cusso et al. 2020). For each strain, two consecutive re-isolations were conducted on Brucella agar at 35 °C under anaerobic conditions for a period of 48 h. A 0.5 McFarland suspension of the *C. difficile* strain was prepared from the cultures, and 200 μ L of the suspension was inoculated into another BHI broth (previously reduced in an anaerobic environment for four days). This was then incubated at 35 °C in anaerobiosis for four days. Following incubation, the broth was vortexed and subsequently centrifuged at 1200 rpm for three minutes. The supernatant was then transferred to an immunoassay extraction buffer and vortexed, and 3 μ L of the mixture were added to the immunoassay device. After 15 min of incubation, the device was read on the F2400 fluorescence reader. This procedure was repeated twice for each of the strains.

Animal model of CDI

CDI was induced in female C57BL/6 mice ($n = 16$) following a protocol comprising 10 days of preconditioning antibiotic in drinking water with cefoperazone 0.5 mg/mL, with water and antibiotic renewed every 48 h, followed by a single dose of 10 mg/kg clindamycin intraperitoneally 1 day before orogastric administration of 10^6 colony-forming units (CFUs) of *C. difficile* ribotype 027 (Cusso et al. 2020). The

concentration of the bacterial inoculum was experimentally confirmed by CFU plating according to McFarland standards. As a control, a different group of animals (n = 14) underwent the same antibiotic treatment to develop a dysbiosis without specific *C. difficile* infection (DWI), caused by disruption of the gut microbiota. In addition, wild-type (WT) animals (n = 14) were used as healthy controls.

The weight and clinical status of the animals were monitored every 2–3 days following the protocol established by Shelby et al. (Shelby et al. 2020), starting from the initiation of antibiotic treatment. The animals were monitored daily after infection or administration of the imaging agent. Clinical CDI was defined as a Clinical Sickness Score (CSS) equal to or greater than 6.

Validation of the CDI animal model

The model was validated by measuring colon length, culturing *C. difficile* from feces, and performing hematoxylin and eosin (H&E)-based histology after in vivo imaging.

The length of the colon was determined by extracting the organ and measuring the total length from the cecum to the rectum with a ruler. Photographs of the colon were taken above the ruler for subsequent analysis.

The concentration of toxigenic *C. difficile* in stool samples was determined based on the procedure described below. Stool samples were weighed and homogenized in vials containing 1 mL of saline solution by using the gentle MACS Dissociator (Miltenyi Biotec) to ensure a uniform mixture. For molecular analysis, 100 μ L of the homogenate from each vial was analyzed using the Xpert™ *C. difficile* assay (GeneXpert, Cepheid, Sunnyvale, California, USA), which detects genes encoding toxin B, binary toxin, and the deletion at position 117 of the *tcdC* gene. This molecular technique was used to confirm that the strain infecting the mice corresponded to the originally administered ribotype 027, which carries this characteristic deletion. For culture analysis, serial 100- μ L dilutions of the homogenate were prepared to achieve 1:1000 and 1:1,000,000 dilutions. A volume of 100 μ L from the undiluted homogenate, as well as from the 10^{-3} and 10^{-6} dilutions, was plated in triplicate on *Clostridium difficile* agar plates (bioMérieux, Marcy-l'Étoile, France)s. All plates were incubated anaerobically at 37 °C for 48 h. Following incubation, TCD colonies were counted and expressed as CFUs per microgram of stool sample.

For H&E-based histological assessment, the bowel specimens were fixed for 24 h in 10% formalin and subsequently dehydrated in 70%, 96% and 100% alcohol and xylene for paraffin-embedding. Paraffin blocks were cut into 4- μ m slices and stained after rehydration with H&E. All samples were evaluated by a pathologist blinded to the experimental groups. Inflammation was scored using a semi-quantitative scale adapted from (Phillips et al. 1992), assessing five key parameters: (I) crypt architecture (normal or altered), (II) chronic inflammation in the lamina propria (graded as mild, moderate, or severe based on the extent of cellular infiltration), (III) acute inflammation (based on the proportion of polymorphonuclear leukocytes among inflammatory cells: < 1/3 = mild, 1/3–2/3 = moderate, > 2/3 = severe), (IV) depth of inflammatory involvement (mucosal, submucosal, muscular, or transmural), and (V) presence or absence of adenomatous changes.

Ex vivo biodistribution of [⁸⁹Zr]Zr-DFO-Beztxab

In order to determine the optimal uptake time for in vivo PET/CT imaging, we conducted ex-vivo biodistribution studies at 48 h and 5 days post-infection.

Animals received [⁸⁹Zr]Zr-DFO-Beztxab (1.11–3.7 MBq in 200 μL of PBS 1×) intravenously 24 h after infection. The animals were then euthanized at their corresponding uptake times, and the organs of interest were harvested. The experimental groups and sample sizes were as follows:

- 48 h post-infection: CDI (n = 4), DWI (n = 4), WT (n = 4).
- 5 days post-infection: CDI (n = 3), DWI (n = 5), WT (n = 5).

The harvested organs included blood, heart, lungs, liver, spleen, kidneys, stomach, colon + cecum, skin, bone, and intestine. Feces was also sampled.

Activity was measured in a Wallac Wizard 1480–011 Automatic Gamma Counter (Revvity, Inc., Waltham, MA, USA) and biodistribution was expressed as mean percentage of injected dose per gram of tissue (%ID/g).

In vivo PET/CT imaging of [⁸⁹Zr]Zr-DFO-Beztxab

PET/CT studies were conducted using a small-animal PET/CT scanner (PET/CT SuperArgus, SEDECAL Molecular Imaging, Madrid, Spain). Twenty-four hours after the infection time-point, the animals (CDI n = 9, DWI n = 5, WT n = 5) received [⁸⁹Zr]Zr-DFO-Beztxab (3.70 MBq in 200 μL of PBS 1×) intravenously. Images were acquired 24 h after radiotracer administration and 48 h post-infection. Before CT acquisition, 0.3 mL of Iopamiro (Bracco, Milan, Italy) was administered intraperitoneally. During acquisition, animals were anesthetized with 1.5% sevoflurane in oxygen (SevoFlo, Zoetis Belgium SA, Louvain-la-Neuve, Belgium). PET data were collected for 30 min and reconstructed using FORE/2D-OSEM with 16 subsets and 1 iteration (voxel size: 0.388 × 0.388 × 0.775 mm). The CT study was acquired using an X-ray beam current of 340 μA and a tube voltage of 40 kVp, and reconstructed using an FDK algorithm (Pascau et al. 2006; Abella et al. 2012).

PET/CT images were analyzed using Multimodality Workstation software (Pascau et al. 2006). On each CT image, a region of interest (ROI) was selected in the peritoneal cavity (Fig. 1) using the kidneys as reference, and delimited by (1) an axial plane just below the most caudal kidney pole and (2) a coronal plane ventral to the kidneys,

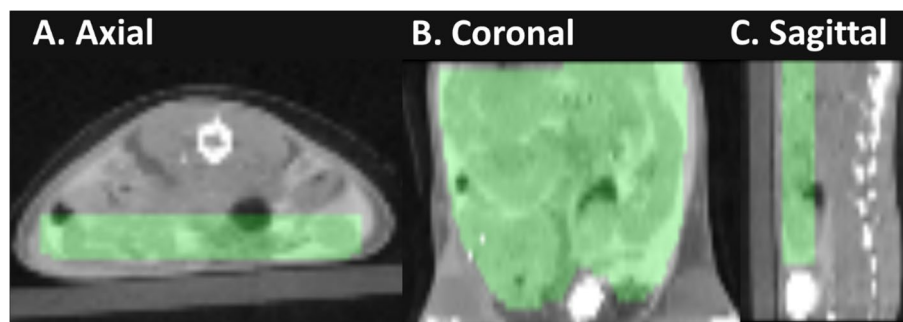


Fig. 1 Abdominal ROI selected for PET quantification, shown in the **A** axial, **B** coronal, and **C** sagittal planes

always avoiding the bladder. These ROIs were automatically applied to co-registered PET images to measure mean standard uptake values in the ROI (SUV_{mean}).

Data processing and statistical analysis

We used Prism 8.3.0 (GraphPad Software, La Jolla, CA, USA) for data processing and plotting. Values are presented as mean \pm standard deviation.

Given that some data did not meet the criteria of normality and homoscedasticity, we used the Kruskal–Wallis test followed by a post hoc Mann–Whitney test for all the variables evaluated. In all cases, the significance threshold was set at $p < 0.05$.

Ethics

C57BL/6 female mice from Charles River were housed in the animal facility of Hospital General Universitario Gregorio Marañón, Madrid, Spain (ES28079000087). All animal procedures conformed to EU Directive 2010/63EU and national regulations (RD 53/2013) and were approved by the local ethics committees and the Animal Protection Board of the Comunidad Autónoma de Madrid (PROEX 244–19).

Results

Synthesis and characterization of the radiotracers [¹²⁵I]-Beztxab and [⁸⁹Zr]Zr-DFO-Beztxab

The radiotracer [¹²⁵I]-Beztxab was synthesized with a radiochemical yield of $75.36 \pm 4.11\%$, a specific activity of 167.24 ± 45.14 MBq/mg and a radiochemical purity of higher than 99.99%, as established by TLC (Fig. 2A).

[⁸⁹Zr]Zr-DFO-Beztxab was synthesized with a radiochemical yield of $71.58 \pm 8.19\%$, a specific activity of 202.76 ± 34.04 MBq/mg and a radiochemical purity of higher than 99.99% (Fig. 3A). The calculated LogP value using [⁸⁹Zr]Zr-DFO-Beztxab was -2.41 ± 0.86 , which is in accordance with hydrophilic behavior.

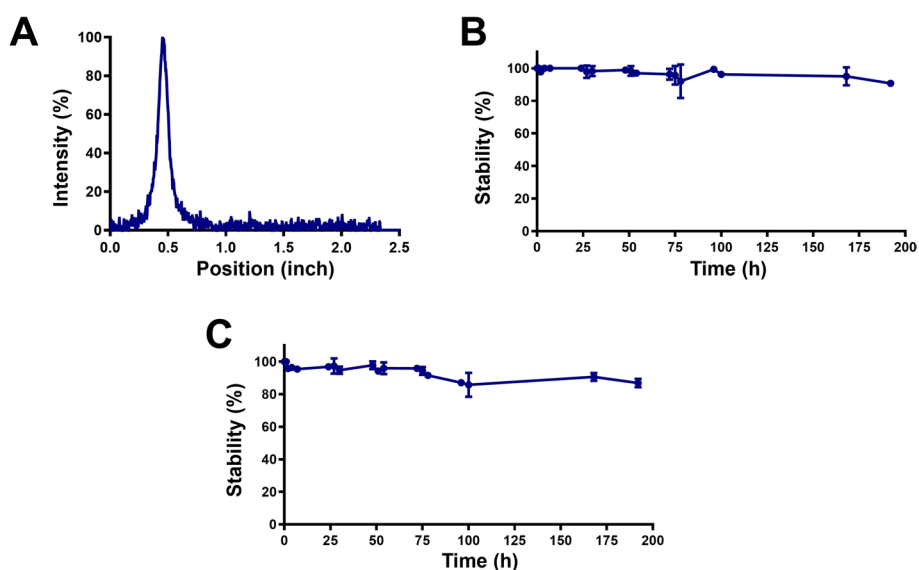


Fig. 2 Characterization of [¹²⁵I]-Beztxab. **A** TLC chromatogram of purified [¹²⁵I]-Beztxab. **B** In vitro stability of [¹²⁵I]-Beztxab in PBS 1 x. **C** In vitro stability of [¹²⁵I]-Beztxab in mouse serum

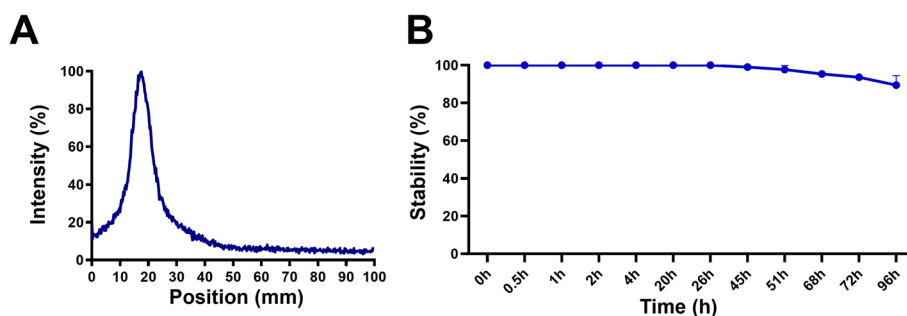


Fig. 3 Characterization of $[^{89}\text{Zr}]\text{Zr-DFO-Beztxab}$. **A** TLC chromatogram of purified $[^{89}\text{Zr}]\text{Zr-DFO-Beztxab}$. **B** In vitro stability of $[^{89}\text{Zr}]\text{Zr-DFO-Beztxab}$ in PBS

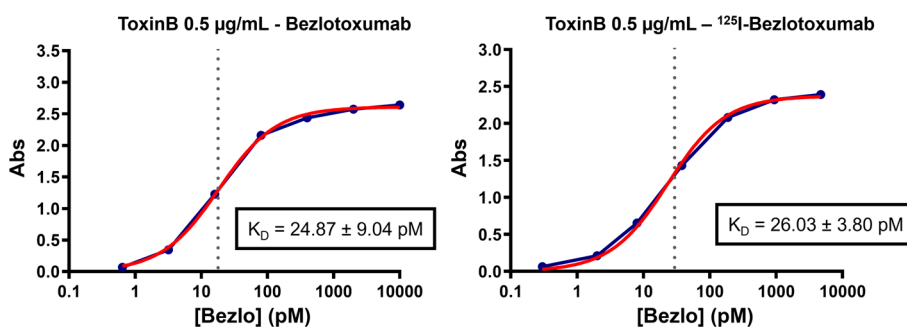


Fig. 4 Determination of the dissociation constant (K_D) of bezlotoxumab and $[^{125}\text{I}]\text{-Beztxab}$ by ELISA. **(Left)** Binding curve of bezlotoxumab to *C. difficile* toxin B. **(Right)** Binding curve of $[^{125}\text{I}]\text{-Beztxab}$ to *C. difficile* toxin B. Data are presented as the mean \pm standard deviation of three independent experiments

In vitro characterization of $[^{125}\text{I}]\text{-Beztxab}$

The in vitro stability of $[^{125}\text{I}]\text{-Beztxab}$ in PBS 1 \times remained at 100% at 24 h and slowly decreased to $90.7 \pm 1.6\%$ at 192 h. Stability in mouse serum remained at 100% after 1 h and slowly decreased to $86.9 \pm 2.6\%$ after 192 h (Fig. 2 B-C). In the case of $[^{89}\text{Zr}]\text{Zr-DFO-Beztxab}$, stability in PBS 1 \times remained at 100% at 26.5 h and slowly decreased to $95.0 \pm 0.6\%$ at 100 h (Fig. 3B).

The K_D of bezlotoxumab and $[^{125}\text{I}]\text{-Beztxab}$ measured by ELISA was 24.87 ± 9.04 and 26.03 ± 3.80 pM, respectively (Fig. 4). The binding kinetic constants measured using LigandTracer were $K_D = 5.22 \pm 1.66$ pM, $k_a = 3.08 \times 10^5 \pm 9.76 \times 10^4$ $\text{M}^{-1} \text{s}^{-1}$, and $k_d = 1.52 \times 10^{-6} \pm 2.87 \times 10^{-7}$ s^{-1} (Fig. 5).

Quantification of toxin expression in *C. difficile* strains

Table 1 shows the results of the *C. difficile* toxin A/B FIA immunoassay. Although this method is mainly qualitative, it offers indirect toxin quantification by providing data in fluorescence units, which serve as a relative measure of the amount of toxins A and B produced by each strain. Based on these measurements, high capacity for production of toxin A was observed for strains ATCC 43255 (ribotype 087) and 14243227 (ribotype 027); high capacity for production of toxin B was observed for ATCC 43255 (ribotype 087), and, especially, strain 14243227 (ribotype 027). As bezlotoxumab binds specifically to toxin B, the latter strain was selected for the animal CDI model.

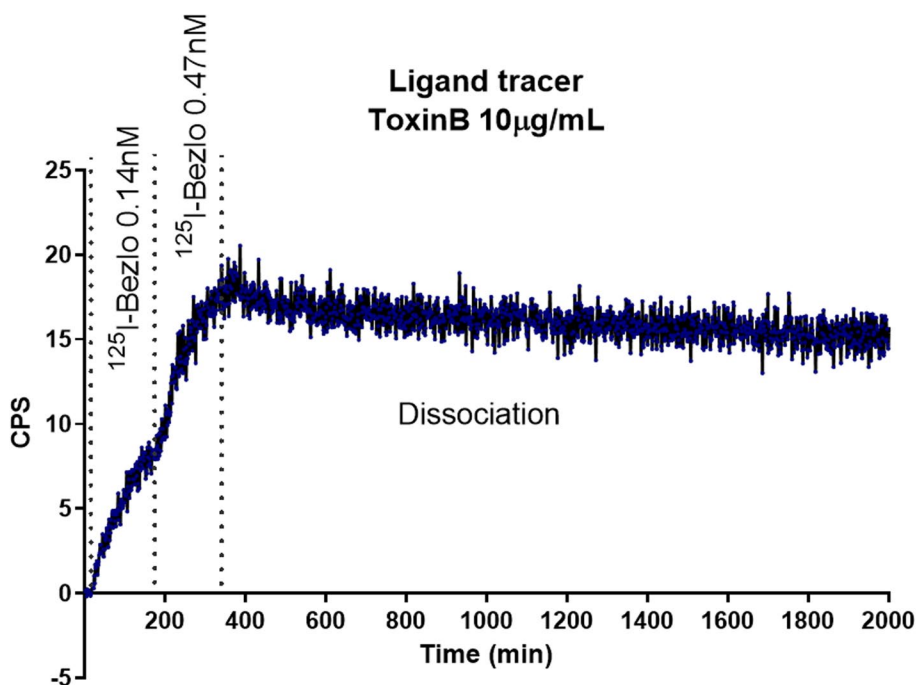


Fig. 5 Binding kinetics of [¹²⁵I]-Beztxab for *C. difficile* toxin B by LigandTracer, showing ligand association and dissociation (expressed as CPS in the targeted toxin B) over time

Table 1 Toxin A/B FIA immunoassay results

Strain	Ribotype	Mean relative toxin production	
		Toxin A	Toxin B
ATCC 43255	087	86.52 ± 0.28	10.62 ± 4.76
14243227	027	86.14 ± 3.05	14.87 ± 11.03
13061479	001	63.31 ± 7.30	0.41 ± 0.04

Validation of the CDI animal model

The CDI animals deteriorated rapidly within 24 h of administration of *C. difficile*. At 24 h post-infection, the CDI group exhibited a cumulative CSS of 25, which increased to 46 at the imaging time-point of 48 h post-infection. In contrast, the DWI and WT groups showed a cumulative CSS of 5 and 2, respectively, at 24 h post-infection, and a cumulative CSS of 6 and 2, respectively, at 48 h post-infection. The ex vivo measurements of colon length demonstrated a significant shortening in the CDI group (5.76 ± 0.40 cm) compared to the DWI (6.80 ± 0.50 cm, p < 0.01) and WT (6.50 ± 0.57 cm, p < 0.05) groups (Fig. 6).

Quantification of toxin from fecal samples was positive for the presence of *C. difficile* in all CDI animals. Quantification of TCD in stool samples was 177.90 ± 284.81 CFU/µg.

The main histopathological lesions were architectural changes in the bowel crypts, increase of lymphocytes and plasma cells in the lamina propria of the bowel, and polymorphonuclear cells in both the lamina propria and the epithelium.

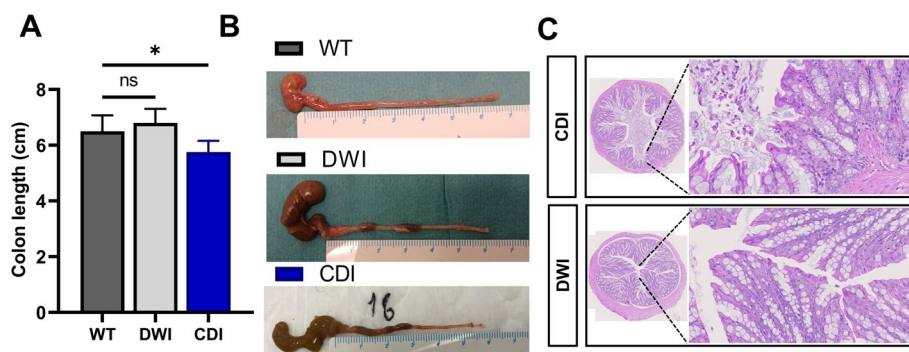


Fig. 6 **A** Ex vivo measurements of colon length of the three animal models. **B** Representative pictures of the measurement of colon length of the three animal models. **C** Representative H&E-based histology of CDI and DWI animal models. The statistical analysis was performed using the Kruskal–Wallis test for independent samples and a post hoc Mann–Whitney test, * $p < 0.05$

Table 2 Ex vivo biodistribution results expressed as %ID/g

	CDI	DWI	WT
48 h p. infection			
Blood	21.46 ± 1.11	27.03 ± 1.47	26.11 ± 2.12
Heart	6.19 ± 0.70	7.43 ± 0.82	8.03 ± 1.75
Lungs	9.25 ± 1.19	12.56 ± 2.15	11.43 ± 1.88
Liver	6.18 ± 0.47	5.93 ± 0.67	6.31 ± 0.63
Spleen	8.53 ± 2.75	6.96 ± 1.53	6.81 ± 1.25
Kidneys	12.23 ± 2.03	11.74 ± 0.47	11.21 ± 1.01
Stomach	3.33 ± 1.38	2.22 ± 0.53	2.76 ± 0.67
Colon + cecum	7.66 ± 5.02	3.43 ± 0.43	3.21 ± 0.78
Skin	3.71 ± 0.78	3.94 ± 1.14	4.99 ± 1.29
Bone	3.50 ± 0.56	3.87 ± 0.64	3.27 ± 0.30
Intestine	3.65 ± 1.68	3.54 ± 0.40	3.76 ± 0.98
Feces	2.71 ± 0.63	1.10 ± 0.52	1.31 ± 0.20
5 d p. infection			
Blood	11.93 ± 2.08	22.57 ± 8.64	20.03 ± 6.66
Heart	6.61 ± 1.97	7.44 ± 1.94	6.86 ± 1.18
Lungs	9.08 ± 4.16	14.45 ± 1.96	14.27 ± 2.86
Liver	6.31 ± 1.72	8.54 ± 4.67	7.84 ± 1.19
Spleen	7.46 ± 2.07	13.10 ± 8.58	9.92 ± 3.17
Kidneys	7.69 ± 2.39	11.07 ± 1.92	11.49 ± 2.05
Stomach	1.57 ± 0.50	1.78 ± 0.52	2.23 ± 0.18
Colon + cecum	4.01 ± 0.88	2.02 ± 1.68	1.99 ± 0.46
Skin	4.65 ± 1.59	6.18 ± 2.00	5.49 ± 0.90
Bone	3.96 ± 0.53	6.81 ± 0.58	7.43 ± 0.80
Intestine	2.10 ± 0.50	3.50 ± 0.50	3.54 ± 1.07
Feces	1.00 ± 0.15	1.79 ± 1.09	1.95 ± 1.00

Ex vivo biodistribution

Table 2 and Fig. 7 present the biodistribution values of [^{89}Zr]Zr-DFO-Beztxab in an independent group of animals (48 h and 5 days of infection). Colon + cecum uptake in CDI animals was 1.9-fold higher at 48 h post-infection ($7.66 \pm 5.02\% \text{ID/g}$) than at

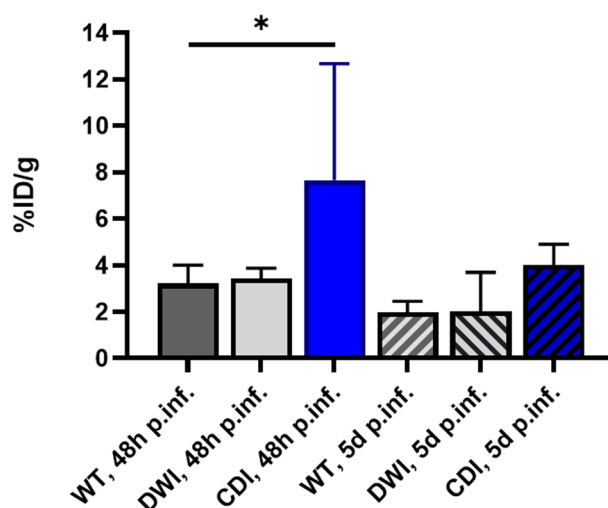


Fig. 7 Biodistribution of [^{89}Zr]Zr-DFO-Beztxab in colon-cecum in the three animal models 48 h and 5 days post-infection (48 h post-infection: CDI n = 4, DWI n = 4, WT n = 4; 5 days post-infection: CDI n = 3, DWI n = 5, WT n = 5). The statistical analysis was performed using the Kruskal–Wallis test for independent samples and a post hoc Mann–Whitney test, *p < 0.05

5 days ($4.01 \pm 0.88\% \text{ID/g}$). Thus, the 48-h time point was chosen for in vivo studies to optimize PET imaging. Colon + cecum uptake at 48 h was significantly higher in CDI animals ($7.66 \pm 5.02\% \text{ID/g}$) than in DWI ($3.43 \pm 0.43\% \text{ID/g}$) and WT animals ($3.21 \pm 0.78\% \text{ID/g}$). Differences between CDI animals and the other groups were lower at 5 days.

In vivo PET/CT imaging of [^{89}Zr]Zr-DFO-Beztxab

Qualitatively, in vivo PET/CT images of [^{89}Zr]Zr-DFO-Beztxab confirmed the existence of specific and localized radiotracer uptake in different segments of the digestive tract. In contrast, the control groups exhibited slight abdominal uptake, basically in excretory organs and the circulatory system, with no apparent accumulation in the digestive system (Fig. 8A, B). Quantification of abdominal uptake (SUVmean) showed an increase in [^{89}Zr]Zr-DFO-Beztxab uptake in infected animals (SUVmean 0.85 ± 0.06 ; $p = 0.003$) compared with WT animals (SUVmean 0.66 ± 0.07) (Fig. 8C).

Discussion

Despite ongoing advancements in identifying infection sites, effective non-invasive detection methods remain scarce. A major challenge lies in differentiating between inflammatory and infectious processes, which can lead to false-positive diagnoses (Rosenbaum et al. 2006). Building on the success of immunoPET imaging in oncology (Menke-Van Der Houven et al. 2019) and our group's previous work in targeting bacterial toxins (González et al. 2024), this study evaluates an immuno-PET tracer using a [^{89}Zr]Zr-radiolabeled antibody targeting *C. difficile* toxin B.

To this end, two different radiolabeling approaches of the monoclonal antibody bezlotoxumab were performed. The [^{125}I]I radiolabeling, with a radioisotope half-life of 59.49 days, enabled long-lasting in vitro binding studies up to 2000 min. Additionally, direct

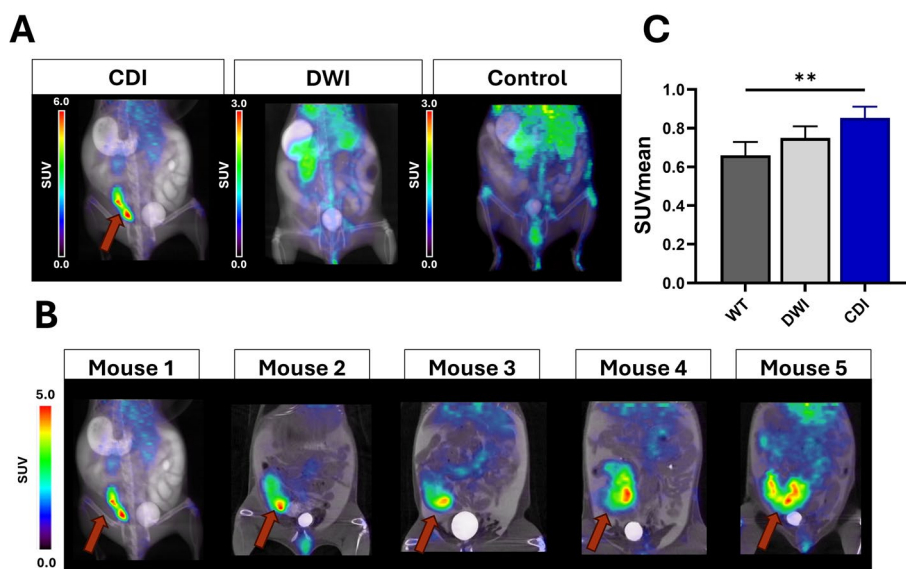


Fig. 8 **A** Representative images of in vivo PET/CT imaging of [^{89}Zr]Zr-DFO-Beztxab in the three animal models 48 h post-infection. The red arrow indicates colon-cecum uptake. **B** Additional images of CDI animal models 48 h post-infection. The red arrows indicate colon-cecum uptake. **C** PET/CT images quantification in the three animal models (CDI $n = 9$, DWI $n = 5$, WT $n = 5$) expressed as SUVmean. The statistical analysis was performed using the Kruskal–Wallis test for independent samples and a post hoc Mann–Whitney test, $**p < 0.01$

radioiodination is a simple, fast and inexpensive reaction, unlike [^{89}Zr]Zr. However, despite its potential for SPECT imaging, its low gamma energy (35 keV) limits its use as an imaging agent (Kim et al. 2015). Following in vitro binding validation with [^{125}I]I, we radiolabeled bezlotoxumab with [^{89}Zr]Zr, a well-established radioisotope used in immunoPET for in vivo PET imaging in humans (Jauw et al. 2019). Its half-life of 78.42 h allows for longitudinal studies while providing more sensitive PET images.

[^{125}I]I radiolabeling was performed with a low amount of radioactivity owing to the long half-life of the radioisotope and the low activity required for in vitro binding assays. This resulted in a good radiochemical yield of $75.36 \pm 4.11\%$ and, consequently, a relatively low specific activity of 167.24 ± 45.14 MBq/mg. The high radiochemical purity of more than 99.99% and the long in vitro stability in PBS ensured that the results obtained in the in vitro binding assays were not caused by the binding of free [^{125}I]I.

Radiolabeling with [^{89}Zr]Zr resulted in a good radiochemical yield of $71.58 \pm 8.19\%$, similar to that of other immunotracers for toxins developed by our group (González et al. 2024). A higher specific activity of 202.76 ± 34.04 MBq/mg was achieved in this case. Even though this value is still relatively low for monoclonal antibodies, it remains in the range of other similar antibodies and in the intended value for small animal imaging (74–222 MBq/mg) (Verel et al. 2003; Wuensche et al. 2022; Sharma et al. 2020). As in the previous case, the radio-chemical purity was higher than 99.99%, and in vitro stability in PBS remained above $95.0 \pm 0.6\%$ at 100 h.

The K_D values of [^{125}I]I-Beztxab determined by ELISA showed a high binding affinity of bezlotoxumab for *C. difficile* B toxins, in the picomolar range (Roskos et al. 2007). A slight increase in the K_D of [^{125}I]I-Beztxab compared to the unlabeled version may indicate a small loss of affinity. However, the standard deviations of the

two values overlap, suggesting that the difference may be due to measurement error. There is a small difference between K_D values measured by ELISA (26.03 ± 3.80 pM) and LigandTracer (5.22 ± 1.66 pM). Compared to ELISA, LigandTracer usually yields lower K_D values because it provides a more reliable result by collecting data over several days with different ligand concentrations, thus enabling the measurement of k_a ($3.08 \times 10^5 \pm 9.76 \times 10^4$ M⁻¹ s⁻¹) and k_d ($1.52 \times 10^{-6} \pm 2.87 \times 10^{-7}$ s⁻¹). Nevertheless, both K_D values are in the picomolar range, demonstrating the high binding affinity of the antibody. The association and dissociation constants also indicate rapid binding and slow release of the antibody to its target, with values approximately ten times higher and lower, respectively, than those of other antibodies (Faresjö et al. 2021; Gustavsson et al. 2020).

Among the *C. difficile* strains evaluated for toxin production, strain 14243227 (ribotype 027) and strain ATCC 43255 (ribotype 087) exhibited the highest relative levels of toxin A production, with strain 14243227 also displaying the highest relative level of toxin B production. Moreover, our previous work using a mouse model with PET/CT imaging and [¹⁸F]F-FDG found higher levels of toxins in animals infected with this strain (Cusso et al. 2020). Bezlotoxumab binds specifically to toxin B; therefore, strain 14243227 was selected for the initial evaluation of a radiotracer based on this antibody, excluding the other strains in order to validate the probe's performance in an optimal scenario. Although it is reasonable to question whether a *C. difficile* strain that produces high levels of toxin B in vitro, such as the one used in this study, will do so in vivo, previous studies involving multiple ribotype 027 strains have demonstrated consistently high in vivo toxin B production (Verdoorn et al. 2010). As this strain also exhibits a relatively high production of toxin A, future studies with different targeting antibodies can be conducted using the same strain.

We used two different animal models, one for *C. difficile* infection and another to develop a dysbiosis without infection (DWI). Dysbiosis, an imbalance in the gut microbiota, is linked to several diseases such as inflammatory bowel disease (Haneishi et al. 2023). We induced dysbiosis using a combination of antibiotics disrupting gut microbiota and favoring *C. difficile* infection (Vasilescu et al. 2022). A healthy gut microbiome usually protects against pathogens through nutrient competition, antimicrobial production, and maintenance of an acidic environment (Minkoff et al. 2023). When disrupted, it allows *C. difficile* to proliferate. The two models selected enabled us to test the radiotracer's ability to differentiate between active infection and inflammatory pathways triggered by dysbiosis.

Animal models were validated in three different ways: (1) The reduction in colon length indicated the existence of inflammation (Zhou et al. 2018). (2) Bacterial cultures from fecal samples confirmed the presence of *C. difficile* in all CDI animals, but not in the rest. Toxin quantification presented high variance (177.90 ± 284.81 CFU/ μ g), which is attributable to the skewed, non-normal distribution of *C. difficile* colonization in vivo, indicative of an exponential growth dynamics of the bacteria, where minor variations in colonization timing or host factors can result in substantial disparities in bacterial burden (Ozaki et al. 2004; Koenigsnecht et al. 2015; De-la-Rosa-Martínez et al. 2025). (3) H&E-based histology confirmed inflammation of the colon, with higher levels in the DWI model. This finding further underscores the capability

of our radiotracer to detect toxin B for diagnosing *C. difficile* infection, while avoiding non-specific uptake by colon inflammation.

Ex vivo biodistribution studies were conducted in the three animal models prior to PET/CT imaging to determine optimal radiotracer uptake time, aiming to identify the best time-point for early diagnosis. Biodistributions were performed at 48 h and 5 days of infection, with 24 h and 4 days of radiotracer uptake, respectively. The uptake in the colon and cecum at 48 h post-infection was found to be 1.9 times higher ($7.66 \pm 5.02\%ID/g$) than the uptake observed at 5 days post-infection ($4.01 \pm 0.88\%ID/g$). Based on this finding, the 48-h time-point was selected for subsequent in vivo PET imaging studies to maximize detection sensitivity. Furthermore, at 48 h post-infection, colon and cecum uptake were significantly higher in CDI animals ($7.66 \pm 5.02\%ID/g$) than in DWI animals ($3.43 \pm 0.43\%ID/g$) and WT controls ($3.21 \pm 0.78\%ID/g$). The smaller difference between DWI or WT and CDI between day 2 and day 5 likely reflects the natural progression of the disease. By day 5, partial resolution of inflammation in the DWI group and faster recovery in mice compared to humans may influence tracer kinetics and clearance (Tomkovich et al. 2020). Lower ex vivo uptake on day 5 supports this trend. These differences suggest that this time frame is optimal for distinguishing active CDI from DWI-driven inflammation and healthy controls.

PET/CT imaging analysis of the CDI animal model clearly showed a distinct and precisely localized uptake pattern for [^{89}Zr]Zr-DFO-Beztxab in different segments of the lower digestive tract. This pattern is typically associated with CDI. Interestingly, DWI and WT models exhibited a markedly different uptake profile, which was localized mainly in excretory organs and the circulatory system, with low accumulation within the gastrointestinal tract. This disparity supports the specificity of the radiotracer uptake in delineating the pathophysiological processes associated with bacterial infection. Uptake in bones and joints is high in all animal models. The reason for this may be demetallization of [^{89}Zr]Zr in DFO-conjugated 150-kDa IgG isotype antibodies in plasma, which is a common issue that has been observed in previous studies (Raavé et al. 2019) and often leads to uptake of free [^{89}Zr]Zr in bone tissue, especially in joints (Abou et al. 2011). This qualitative analysis of the images is supported by the quantitative analysis, where abdominal uptake was more pronounced in the infected group than in the WT and DWI animals. The fact that we observed colonic PET uptake even with low levels of TCD may suggest a higher sensitivity of PET, although this speculation would require further confirmation.

Our study is subject to limitations. First, the sample size for the ex vivo biodistribution analysis performed 5 days post-infection was insufficient to obtain statistically significant results, although the trend suggested higher uptake in the colon of CDI animals. Second, only one strain of *C. difficile* (ribotype 027) was used, namely, the one that demonstrated the highest level of toxin B production among the evaluated strains. While this choice facilitated radiotracer validation in an optimal scenario, future studies should evaluate tracer performance on strains with lower toxin B production to determine a more realistic detection limit. Third, PET image quantification was performed using an abdominal ROI rather than a more specific colonic and cecal ROI owing to challenges in differentiating these organs on CT images. This lack of specificity may have affected the accuracy of uptake measurements. In addition, the study was conducted in a mouse model, which,

while useful for preclinical evaluation, does not fully replicate the complexity of human CDI. Differences in immune response, gut microbiota composition, and toxin distribution between mice and humans may limit the direct translation of findings to clinical practice (Best et al. 2012). Fourth, no attempt was made to detect *C. difficile* outside the gastrointestinal tract. Finally, the study did not evaluate potential cross-reactivity with other gut bacteria or inflammatory conditions, potentially affecting the specificity of the tracer in clinical settings. These limitations should be addressed in future research to refine the diagnostic accuracy and translational potential of this immunoPET approach.

While not intended to replace current diagnostic algorithms for CDI, this immunoPET radiotracer may serve as a valuable complementary tool to enhance diagnosis and foresee patient prognosis. The ability to non-invasively detect CDI in early stages represents a significant advancement over invasive techniques such as colonoscopy, which carries substantial risks in severely ill patients (McDonald et al. 2018). Early detection would allow for timely intervention, potentially reducing disease progression and severe complications such as pseudomembranous colitis and toxic megacolon (Rajack et al. 2023). Although our work focuses on the acute phase (2–3 days post-infection), the design of the tracer opens the possibility of detecting the disease at earlier stages, since toxin production may begin before any macroscopic endoscopic lesions appear. However, claiming an early detection (even before the onset of symptoms or diarrhea) was out of the scope of our study and would require additional studies. The radiotracers also enable specific visualization of toxin-producing bacterial foci in vivo, which may be important for precise differentiation between active infection and colonization. This could be particularly advantageous in complex clinical scenarios, such as patients with coexisting gastrointestinal disorders or recurrent CDI, where misdiagnosis can lead to unnecessary treatment or delayed care. Recurrent CDI remains a major challenge, often requiring repeated and prolonged courses of therapy (Finn et al. 2021). The proposed radiotracer could identify residual infection sites and differentiate recurrent infection from post-treatment inflammatory changes, reducing the reliance on empirical therapy and potentially curbing antimicrobial resistance associated with overuse of broad-spectrum antibiotics. Additionally, the ability to monitor the response to therapy in vivo would enable clinicians to adjust treatments dynamically, potentially improving patient outcomes. Finally, this immunoPET approach could be used as a non-invasive tool in clinical trials to quantify reductions in radiotracer uptake over time (an indicator of decreased toxin B activity) providing a direct measure of treatment efficacy against CDI.

Conclusions

We synthesized and characterized two *C. difficile*-specific radiotracers based on bezlotoxumab. Radiolabeling with both [¹²⁵I]I and [⁸⁹Zr]Zr was successfully achieved with a high radiochemical yield, purity, and stability, thus supporting the use of these radiotracers for in vivo assessments. In vitro binding assays using [¹²⁵I]I-Beztxab confirmed high and rapid uptake of bezlotoxumab, with slow release even at long time-points. PET/CT imaging using [⁸⁹Zr]Zr-DFO-Beztxab revealed distinct and specific uptake in the digestive tract of CDI animals, but not in the other groups. These findings support the radiotracer's ability to differentiate between active infection and dysbiosis without specific *C. difficile* infection, providing valuable evidence of its diagnostic potential.

Abbreviations

[¹²⁵ I]-Beztxab	[¹²⁵ I]-radiolabeled bezlotoxumab
[¹⁸ F]F-FDG	[¹⁸ F]F-fluorodeoxyglucose
[⁸⁹ Zr]Zr-DFO-Beztxab	[⁸⁹ Zr]Zr-radiolabeled bezlotoxumab
DWI	Dysbiosis without specific <i>C. difficile</i> infection
<i>C. difficile</i>	<i>Clostridioides difficile</i>
CDI	<i>Clostridioides difficile</i> infection
CFU	Colony-forming units
CT	Computed tomography
EIA	Enzyme immunoassay
ELISA	Enzyme-linked immunosorbent assay
GDH	Glutamate dehydrogenase
H&E	Hematoxylin and Eosin
PBS	Phosphate-buffered saline
PET	Positron emission tomography
p-NCS-Bz-DFO	p-Isothiocyanatobenzyl-deferoxamine
ROI	Region of interest
SPECT	Single photon emission computed tomography
TCD	Toxicogenic <i>C. difficile</i>
WT	Wild-type

Acknowledgements

The authors thank Diego Eguibar from the Imaging Laboratory for Small Animal Experimentation of Instituto de Investigación Sanitaria Gregorio Marañón for their excellent work with animal preparation and imaging protocols.

Author contributions

MGA and LC contributed equally to this work, performing the main experiments, data analysis and drafting the manuscript. LA quantified *C. difficile* toxin for the different strains and the analysis of stool samples to determine the presence of toxigenic species. MIG assisted in the synthesis of the radiotracer and ex vivo biodistribution studies. AdF performed the animal model and imaging protocols. MJFA performed the H&E staining of colon tissues and their subsequent analysis. DS and SS provided the ¹²⁵I radioisotope and directed its radiolabeling and characterization, including ELISA and ligand tracer assays. EB and PM provided the *C. difficile* background and opportunity for new diagnostic tools. MD helped with experimental design and interpretation of results. Finally, Dr. BS developed the experimental design and interpretation of the results and supervised the work. All the authors read and approved the final manuscript.

Funding

The authors thank Fundación Ramón Areces for their support. This work was funded by Instituto de Salud Carlos III (ISCIII) through projects "PT23/00027" and "PI23/01405", and co-funded by the European Union. The work was also supported by Comunidad de Madrid, project S2022/BMD-7403 (RENIM-CM). The CNIC is supported by the Instituto de Salud Carlos III (ISCIII), the Ministerio de Ciencia, Innovación y Universidades (MICIU), and the Pro CNIC Foundation and is a Severo Ochoa Center of Excellence (grant CEX2020-001041-S funded by MICIU/AEI/10.13039/501100011033). Grant PTA2022-021556-I was funded by MICIU/AEI/10.13039/501100011033 and by FSE +.

Availability of data and materials

The datasets supporting the conclusions of this article are included within the article. The data that support the findings of this study are available from the corresponding author upon reasonable request.

Declarations**Ethics approval and consent to participate**

C57BL/6 female mice from Charles River were housed in the animal facility of Hospital General Universitario Gregorio Marañón, Madrid, Spain (ES280790000087). All animal procedures conformed to EU Directive 2010/63EU and national regulations (RD 53/2013) and were approved by the local ethics committees and the Animal Protection Board of the Comunidad Autónoma de Madrid (PROEX 244–19).

Consent for publication

Not applicable.

Competing interests

The authors declare that they have no known competing financial interests or personal relationships that could have appeared to influence the work reported in this paper.

Author details

¹Unidad de Medicina y Cirugía Experimental, Hospital General Universitario Gregorio Marañón, Instituto de Investigación Sanitaria Gregorio Marañón, 28007 Madrid, Spain. ²Centro Nacional de Investigaciones Cardiovasculares (CNIC), Unidad de Imagen Avanzada, 28029 Madrid, Spain. ³CIBER de Salud Mental, Instituto de Salud Carlos III, Madrid, Spain. ⁴Clinical Microbiology and Infectious Diseases, Hospital General Universitario Gregorio Marañón, Madrid, Spain. ⁵Centro de Investigación Biomédica en Red de Enfermedades Respiratorias (CIBERES), 28029 Madrid, Spain. ⁶Medicine Department, Faculty of Medicine, Universidad Complutense de Madrid, Madrid, Spain. ⁷Servicio de Anatomía Patológica Hospital Clínico San Carlos, Fundación Para la Investigación Biomédica HCSC, 28040 Madrid, Spain. ⁸Department of Public Health and Caring Sciences, Molecular Geriatrics/Rudbeck Laboratory, Uppsala University, 751 85 Uppsala, Sweden.

⁹Department of Bioengineering, Universidad Carlos III de Madrid, 28911 Madrid, Spain. ¹⁰Legal Medicine, Psychiatry and Pathology, Faculty of Medicine, Universidad Complutense de Madrid, Madrid, Spain.

Received: 27 March 2025 Accepted: 7 May 2025

Published online: 13 June 2025

References

- Abella M, Vaquero JJ, Sisniega A, Pascau J, Udías A, García V, Vidal I, Desco M. Software architecture for multi-bed FDG-based reconstruction in X-ray CT scanners. *Comput Methods Programs Biomed.* 2012;107(2):218–32.
- Abou DS, Ku T, Smith-Jones PM. In vivo biodistribution and accumulation of 89Zr in mice. *Nucl Med Biol.* 2011;38(5):675–81.
- Alberto S, Ordonez AA, Arjun C, Aulakh GK, Beziere N, Dadachova E, Ebenhan T, Granados U, Korde A, Jallilian A. The development and validation of radiopharmaceuticals targeting bacterial infection. *J Nucl Med.* 2023;64(11):1676–82.
- Bertagna F, Bisleri G, Motta F, Merli G, Cossalter E, Lucchini S, Biasiotti G, Bosio G, Terzi A, Muneretto C. Possible role of F18-FDG-PET/CT in the diagnosis of endocarditis: preliminary evidence from a review of the literature. *Int J Cardiovasc Imaging.* 2012;28:1417–25.
- Best EL, Freeman J, Wilcox MH. Models for the study of *Clostridium difficile* infection. *Gut Microbes.* 2012;3(2):145–67.
- Bocchetti M, Ferraro MG, Melisi F, Grisolia P, Scrima M, Cossu AM, Yau TO. Overview of current detection methods and micro-RNA potential in *Clostridioides difficile* infection screening. *World J Gastroenterol.* 2023;29(22):3385.
- Casali M, Lauri C, Altini C, Bertagna F, Cassarino G, Cistaro A, Erba AP, Ferrari C, Mainolfi CG, Palucci A. State of the art of 18F-FDG PET/CT application in inflammation and infection: a guide for image acquisition and interpretation. *Clin Transl Imaging.* 2021;9(4):299–339.
- Cho JM, Pardi DS, Khanna S, editors. Update on treatment of *Clostridioides difficile* infection. *Mayo Clinic Proceedings*; 2020: Elsevier
- Crobach M, Dekkers O, Wilcox M, Kuijper E. European society of clinical microbiology and infectious diseases (ESCMID): data review and recommendations for diagnosing *Clostridium difficile*-infection (CDI). *Clin Microbiol Infect.* 2009;15(12):1053–66.
- Cusso L, Reigadas E, Munoz P, Desco M, Bouza E. Evaluation of *Clostridium difficile* infection with PET/CT imaging in a mouse model. *Mol Imag Biol.* 2020;22:587–92.
- Czepiel J, Drózd M, Pituch H, Kuijper EJ, Perucki W, Mielimonka A, Goldman S, Wultańska D, Garlicki A, Biesiada G. *Clostridium difficile* infection. *Eur J Clin Microbiol Infect Dis.* 2019;38:1211–21.
- De-la-Rosa-Martínez D, Villaseñor-Echavarrí R, Vilar-Compte D, Mosqueda-Larrauri V, Zinser-Peniche P, Blumberg S. Heterogeneity of *Clostridioides difficile* asymptomatic colonization prevalence: a systematic review and meta-analysis. *Gut Pathogens.* 2025;17(1):6.
- Faresjö R, Bonvicini G, Fang XT, Aguilar X, Sehlin D, Syvänen S. Brain pharmacokinetics of two BBB penetrating bispecific antibodies of different size. *Fluids Barriers CNS.* 2021;18(1):26.
- Finn E, Andersson FL, Madin-Warburton M. Burden of *Clostridioides difficile* infection (CDI)-a systematic review of the epidemiology of primary and recurrent CDI. *BMC Infect Dis.* 2021;21(1):456.
- Frickenstein AN, Jones MA, Behkam B, McNally LR. Imaging inflammation and infection in the gastrointestinal tract. *Int J Mol Sci.* 2019;21(1):243.
- Fujitani S, George WL, Murthy AR. Comparison of clinical severity score indices for *Clostridium difficile* infection. *Infect Control Hosp Epidemiol.* 2011;32(3):220–8.
- Gilligan PH. Is a two-step glutamate dehydrogenase antigen-cytotoxicity neutralization assay algorithm superior to the premier toxin A and B enzyme immunoassay for laboratory detection of *Clostridium difficile*? *J Clin Microbiol.* 2008;46(4):1523–5.
- González MI, González-Arjona M, Cusso L, Morcillo MÁ, Aguilera-Correa JJ, Esteban J, Kestler M, Calle D, Cerón C, Cortes-Canteli M. In vivo detection of *Staphylococcus aureus* infections using radiolabeled antibodies specific for bacterial toxins. *Int J Biomed Imaging.* 2024;2024(1):3655327.
- Guerri S, Danti G, Frezzetti G, Lucarelli E, Pradella S, Miele V. *Clostridium difficile* colitis: CT findings and differential diagnosis. *Radiol Med (Torino).* 2019;124:1185–98.
- Gustavsson T, Syvänen S, O'Callaghan P, Sehlin D. SPECT imaging of distribution and retention of a brain-penetrating bispecific amyloid- β antibody in a mouse model of Alzheimer's disease. *Transl Neurodegener.* 2020;9(1):37.
- Gustavsson T, Metzendorf NG, Wik E, Roshanbin S, Julku U, Chourlia A, Nilsson P, Andersson KG, Laudon H, Hultqvist G. Long-term effects of immunotherapy with a brain penetrating A β antibody in a mouse model of Alzheimer's disease. *Alzheimer's Res Therapy.* 2023;15(1):90.
- Haneishi Y, Furuya Y, Hasegawa M, Picarelli A, Rossi M, Miyamoto J. Inflammatory bowel diseases and gut microbiota. *Int J Mol Sci.* 2023;24(4):3817.
- Ishimori T, Saga T, Mamede M, Kobayashi H, Higashi T, Nakamoto Y, Sato N, Konishi J. Increased 18F-FDG uptake in a model of inflammation: concanavalin A-mediated lymphocyte activation. *J Nucl Med.* 2002;43(5):658–63.
- Jauw YW, O'Donoghue JA, Zijlstra JM, Hoekstra OS, Menke-Van Der Houven CW, Morschhauser F, Carrasquillo JA, Zweegman S, Pandit-Taskar N, Lammertsma AA. 89Zr-Immuno-PET: toward a noninvasive clinical tool to measure target engagement of therapeutic antibodies in vivo. *J Nucl Med.* 2019;60(12):1825–32.
- Kim YJ, Lim I, Yu AR, Kim BI, Choi CW, Lim SM, Kim JS. Comparative study of imaging characteristics of i-125 imaging using the Siemens Inveon scanner and Siemens Symbia TruePoint. *J Biomed Sci Eng.* 2015;8(10):674–83.
- Koenigsnecht MJ, Theriot CM, Bergin IL, Schumacher CA, Schloss PD, Young VB. Dynamics and establishment of *Clostridium difficile* infection in the murine gastrointestinal tract. *Infect Immun.* 2015;83(3):934–41.
- McDonald LC, Gerding DN, Johnson S, Bakken JS, Carroll KC, Coffin SE, Dubberke ER, Garey KW, Gould CV, Kelly C. Clinical practice guidelines for *Clostridium difficile* infection in adults and children: 2017 update by the infectious diseases society of America (IDSA) and Society for healthcare epidemiology of America (SHEA). *Clin Infect Dis.* 2018;66(7):e1–48.

- Menke-Van Der Houven CW, McGeoch A, Bergstrom M, McSherry I, Smith DA, Cleveland M, Al-Azzam W, Chen L, Verheul H, Hoekstra OS. Immuno-PET imaging to assess target engagement: experience from 89Zr-anti-HER3 mAb (GSK2849330) in patients with solid tumors. *J Nucl Med*. 2019;60(7):902–9.
- Minkoff NZ, Aslam S, Medina M, Tanner-Smith EE, Zackular JP, Acra S, Nicholson MR, Imdad A. Fecal microbiota transplantation for the treatment of recurrent *Clostridioides difficile* (Clostridium difficile). *Cochrane Database Syst Rev*. 2023. <https://doi.org/10.1002/14651858.CD013871.pub2>.
- Novak-Weekley SM, Marlowe EM, Miller JM, Cumpio J, Nomura JH, Vance PH, Weissfeld A. *Clostridium difficile* testing in the clinical laboratory by use of multiple testing algorithms. *J Clin Microbiol*. 2010;48(3):889–93.
- Ozaki E, Kato H, Kita H, Karasawa T, Maegawa T, Koino Y, Matsumoto K, Takada T, Nomoto K, Tanaka R. *Clostridium difficile* colonization in healthy adults: transient colonization and correlation with enterococcal colonization. *J Med Microbiol*. 2004;53(2):167–72.
- Paláu-Dávila L, Lara-Medrano R, Negreros-Osuna AA, Salinas-Chapa M, Garza-González E, Gutierrez-Delgado EM, Camacho-Ortiz A. Efficacy of computed tomography for the prediction of colectomy and mortality in patients with *Clostridium difficile* infection. *Ann Med Surg*. 2016;12:101–5.
- Pascou J, Vaquero JJ, Abella M, Cacho R, Lage E, Desco M. Multimodality workstation for small animal image visualization and analysis. *Mol Imaging Biol*. 2006;8(2):97–8.
- Phillips JD, Kim CS, Fonkalsrud EW, Zeng H, Dindar H. Effects of chronic corticosteroids and vitamin A on the healing of intestinal anastomoses. *Am J Surg*. 1992;163(1):71–7.
- Price EW, Carnazza KE, Carlin SD, Cho A, Edwards KJ, Sevak KK, Glaser JM, de Stanchina E, Janjigian YY, Lewis JS. 89Zr-DFO-AMG102 immuno-PET to determine local hepatocyte growth factor protein levels in tumors for enhanced patient selection. *J Nucl Med*. 2017;58(9):1386–94.
- Raavé R, Sandker G, Adumeau P, Jacobsen CB, Mangin F, Meyer M, Moreau M, Bernhard C, Da Costa L, Dubois A. Direct comparison of the in vitro and in vivo stability of DFO, DFO* and DFOcyclo* for 89 Zr-immunoPET. *Eur J Nucl Med Mol Imaging*. 2019;46:1966–77.
- Rajack F, Medford S, Naab T. *Clostridioides difficile* infection leading to fulminant colitis with toxic megacolon. *Autops Case Rep*. 2023;13: e2023457.
- Rose AN, Baggs J, Kazakova SV, Guh AY, Sarah HY, McCarthy NL, Jernigan JA, Reddy SC. Trends in facility-level rates of *Clostridioides difficile* infections in US hospitals, 2019–2020. *Infect Control Hosp Epidemiol*. 2023;44(2):238–45.
- Rosenbaum SJ, Lind T, Antoch G, Bockisch A. False-positive FDG PET uptake— the role of PET/CT. *Eur Radiol*. 2006;16:1054–65.
- Roskos L, Klakamp S, Liang M, Arends R, Green L. Molecular engineering II: antibody affinity. In: *Handbook of therapeutic antibodies*. Wiley; 2007. p. 145–69.
- Sharma SK, Glaser JM, Edwards KJ, Khozeimeh Sarbisheh E, Salih AK, Lewis JS, Price EW. A systematic evaluation of antibody modification and 89Zr-radiolabeling for optimized immuno-PET. *Bioconjug Chem*. 2020;32(7):1177–91.
- Shelby RD, Tengberg N, Conces M, Olson JK, Navarro JB, Bailey MT, Goodman SD, Besner GE. Development of a standardized scoring system to assess a murine model of *Clostridium difficile* colitis. *J Invest Surg*. 2020;33(10):887–95.
- Szabó S, Feier B, Capatina D, Tertis M, Cristea C, Popa A. An overview of healthcare associated infections and their detection methods caused by pathogen bacteria in Romania and Europe. *J Clin Med*. 2022;11(11):3204.
- Tomkovich S, Stough JM, Bishop L, Schloss PD. The initial gut microbiota and response to antibiotic perturbation influence *Clostridioides difficile* clearance in mice. *Mosphere*. 2020. <https://doi.org/10.1128/msphere.00869-20>.
- Vasilescu I-M, Chifiriuc M-C, Pircalabioru GG, Filip R, Bolocan A, Lazăr V, Dițu L-M, Bleotu C. Gut dysbiosis and *Clostridioides difficile* infection in neonates and adults. *Front Microbiol*. 2022;12: 651081.
- Verdoorn BP, Orenstein R, Rosenblatt JE, Sloan LM, Schleck CD, Harmsen WS, Nyre LM, Patel R. High prevalence of tcdC deletion-carrying *Clostridium difficile* and lack of association with disease severity. *Diagn Microbiol Infect Dis*. 2010;66(1):24–8.
- Verel I, Visser GW, Boellaard R, Stigter-van Walsum M, Snow GB, Van Dongen GA. 89Zr immuno-PET: comprehensive procedures for the production of 89Zr-labeled monoclonal antibodies. *J Nucl Med*. 2003;44(8):1271–81.
- Viprey VF, Davis GL, Benson AD, Ewin D, Spittal W, Vernon JJ, Rupnik M, Banz A, Allantaz F, Cleuziat P. A point-prevalence study on community and inpatient *Clostridioides difficile* infections (CDI): results from combatting bacterial resistance in Europe CDI (COMBACTE-CDI), July to November 2018. *Eurosurveillance*. 2022;27(26):2100704.
- Vosjan MJ, Perk LR, Visser GW, Budde M, Jurek P, Kiefer GE, Van Dongen GA. Conjugation and radiolabeling of monoclonal antibodies with zirconium-89 for PET imaging using the bifunctional chelate p-isothiocyanatobenzyl-desferrioxamine. *Nat Protoc*. 2010;5(4):739–43.
- Wang E, Björkelund H, Mihaylova D, Hagemann UB, Karlsson J, Malmqvist M, Buijs J, Abrahamsén L, Andersson K. Automated functional characterization of radiolabeled antibodies: a time-resolved approach. *Nucl Med Commun*. 2014;35(7):767–76.
- Wilcox MH, Gerding DN, Poxton IR, Kelly C, Nathan R, Birch T, Cornely OA, Rahav G, Bouza E, Lee C. Bezlotoxumab for prevention of recurrent *Clostridium difficile* infection. *N Engl J Med*. 2017;376(4):305–17.
- Wuensche TE, Stergiou N, Mes I, Verlaan M, Schreurs M, Kooijman EJ, Janssen B, Windhorst AD, Jensen A, Asuni AA. Advancing 89Zr-immuno-PET in neuroscience with a bispecific anti-amyloid-beta monoclonal antibody—the choice of chelator is essential. *Theranostics*. 2022;12(16):7067.
- Zeglis BM, Lewis JS. The bioconjugation and radiosynthesis of 89Zr-DFO-labeled antibodies. *JoVE (j vis Exp)*. 2015;96: e52521.
- Zhou F, Hamza T, Fleur AS, Zhang Y, Yu H, Chen K, Heath JE, Chen Y, Huang H, Feng H. Mice with inflammatory bowel disease are susceptible to *Clostridium difficile* infection with severe disease outcomes. *Inflamm Bowel Dis*. 2018;24(3):573–82.

Publisher's Note

Springer Nature remains neutral with regard to jurisdictional claims in published maps and institutional affiliations.